Building Technology and Urban Systems

Lawrence Berkeley National Laboratory

PREDICTING THERMAL TRANSMITTANCE OF VACUUM INSULATING GLAZING UNITS – CENTER OF GLAZING

Cenk Kocer[1], D. Charlie Curcija, Robert G. Hart, Simon Vidanovic

September 22, 2025

[1] University of Sydney

This page intentionally left blank

Disclaimer

Copyright Notice

PREDICTING THERMAL TRANSMITTANCE OF VACUUM INSULATING GLAZING UNITS – CENTER OF GLAZING

Cenk Kocer[1]

D. Charlie Curcija

Robert G. Hart

D. Simon Vidanovic

Ernest Orlando Lawrence Berkeley National Laboratory

1 Cyclotron Road, MS 90R4000

Berkeley CA 94720-8136

August 21, 2025

[1]University of Sydney

Table of Contents

Acronyms and Abbreviations

VIG Vacuum Insulating Glazing

GHP Guarded Hot Plate

FEM Finite Element Method

TAC Thermal Accommodation Coefficient

Nomenclature

A	area [m^2]
C_{pa}	Thermal conductance of the array of support pillars [$W/(m^2 \cdot K)$]
C_{rad}	Glass surface-to-surface thermal radiation conductance [$W/(m^2 \cdot K)$]
C_{cond}	Thermal conductance of the residual low-pressure gas [$W/(m^2 \cdot K)$]
C_{gap}	Thermal conductance of the VIG gap [$W/(m^2 \cdot K)$]
C_{pillar}	The thermal conductance of the residual low-pressure gas [$W/(m^2 \cdot K)$]
C^*	Thermal conductance of the pillars and the residual gas only [$W/(m^2 \cdot K)$]
D	diameter of linear bearing [m]
f	fraction of material remaining in an annulus geometry [-]
h	height of pillar [m]
h_c	Convective surface heat transfer coefficient [$W/(m^2 \cdot K)$]
J	Radiant heat flux leaving the surface [$W/(m^2 \cdot K)$]
k_g	Layer conductivity [$W/(m \cdot K)$]
k_{glass1}, k_{glass2}	thermal conductivity of glass pane 1 and 2 [$W/(m \cdot K)$]
k_{pillar}	thermal conductivity of the pillar material [$W/(m \cdot K)$]
K_1	complete elliptical integral of the first kind [-]
L	length of contact [m]
M	Specific Molecular Weight [mol/g, or kmol/kg]
P	Pressure of the gas [Pa]
R_c	constriction thermal resistance [$m^2 \cdot K/W$]
R_s	spreading thermal resistance [$m^2 \cdot K/W$]
R_d	pillar conduction thermal resistance [$m^2 \cdot K/W$]
R_i	Thermal resistance of the air film on indoor VIG side [$m^2 \cdot K/W$]
R_{gap}	Thermal resistance of the VIG gap [$m^2 \cdot K/W$]

R_{glass1}	Thermal resistance of glass pane 1 [m²·K/W]
R_{glass2}	Thermal resistance of glass pane 3 [m²·K/W]
R_o	Thermal resistance of the air film on outdoor VIG side [m²·K/W]
R_p	total pillar thermal resistance [m²·K/W]
R_{pa}	total pillar array thermal resistance [m²·K/W]
r	cylindrical contact radius [m]
r_1	truncated cone side 1 contact radius [m]
r_2	truncated cone side 2 contact radius [m]
r_i	inner radius of annulus contact [m]
r_o	outer radius of annulus contact [m]
$\Re$	Universal gas constant [J/(mol·K), kJ/(kmol·K) or]
S_p	separation between pillars [m]
t_g	Layer thickness [m]
T	Surface temperature [K]
T_m	Mean temperature between surfaces 2 and 3 [K]
q_{gl}	Heat flux across the solid layer [W/m²]
q_i	Heat flux across the i^{th} gap [W/m²]
q_{i+1}	Heat flux across the $i+1^{th}$ gap [W/m²]
W	width of contact [m]
□	the accommodation coefficient of the gas interaction at the glass surfaces [-]
ε	emissivity of the glass surface [-]
□	Specific heat ratio [-]
ρ	Reflectance [-]
σ	Stefan-Boltzmann Constant 5.67 x 10^{-8}, [W/(m²·K⁴)]
τ	Transmittance [-]
2	surface number 2 [-]
3	surface number 3 [-]
f	*Front* surface [-]
b	*Back* surface [-]
$,i$	i^{th} surface [-]

1. Introduction and Background

Vacuum Insulated Glass (VIG), or sometimes referred to as Evacuated Glazing Units (EGU), is an emerging technology that was developed as a concept ~35 years ago, but only recently approaching widespread commercialization and acceptance. When the first prototype VIG was developed at the University of Sydney, it was released with the thermal model of heat transfer in evacuated space as a function of the pressure (vacuum level), and conduction through small diameter highly conducting cylindrical pillars. In recent years several companies have started experimenting with different pillar geometry and materials, so there was a need to update mathematical models for predicting the thermal performance of VIG excluding contributions from the edge seal (that is, the "center-of-glass" performance). In this document we present: 1) newly updated analytical models for predicting with large selection of pillar geometries and properties; and 2) also present a model for calculating thermal performance from the measured thermal conductivity of the VIG. When using the second model the conductance of the vacuum space, including pillar effects, is calculated without the need to know any details about the vacuum space between glazing layers. This conductance can then be used for pairing glazing layers that are different from the configuration of the original measured unit.

The following figure is a schematic representation of a VIG, where the labeling of the glass layers, and surface numbering, are used throughout this document:

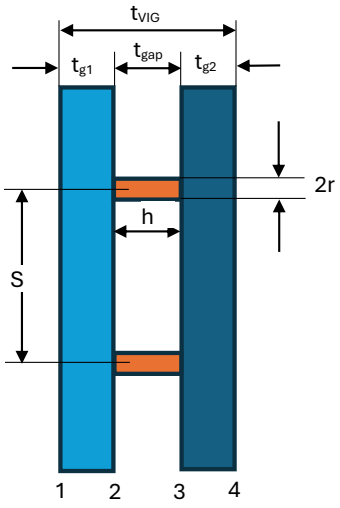

Figure 1. A schematic of the VIG, with the labeling as given, used throughout this document, as a matter of consistency.

2. Thermal Conductance of the VIG Gap

The thermal Conductance of the space between the glass panes, the vacuum gap, C_{gap}, is the sum of the conductance of the; 1. residual low-pressure gas C_{cond}; 2. array of glass support elements (pillars) C_{pa}; and 3. surface-to-surface radiation heat transfer between the glass surfaces in the gap C_{rad}, which is written as,

$$C_{gap} = C_{cond} + C_{pa} + C_{rad} \tag{2.1}$$

where:

C_{gap} = Combined heat conductance of VIG gap space [W/m²K]

C_{cond} = Residual low pressure gas conductance [W/m²K]

C_{pa} = Conductance of the array of support pillars [W/m²K]

C_{rad} = Glass surface-to-surface radiation conductance [W/m²K]

It will be shown later that it is useful to define a subset of thermal conductance, which is the combination of the residual low-pressure gas and the array of support pillars, and is labeled as *C**. This quantity, *C**, is more easily incorporated into the typical overall model of the glazing thermal performance calculation (Curcija et al., 2018). The fundamental definition gives,

$$C^* = C_{cond} + C_{pa} \tag{2.2}$$

In this form, the equation is useful when calculating the overall VIG performance using measurement data, which is accurate since the surface-to-surface radiative calculation is the most accurate and well defined (see Section 4 for full details). This allows us to use this fixed quantity and combine with any combination of glazing layers and can serve as a validation point between measurements and pure calculations.

In the following sections, the detailed analytical solutions for each of the heat flow contributions are outlined. In each case the validation of the analytical solution, with relevant case study results provided where available, are presented.

2.1 Conductance of the Residual Low-Pressure Gas (C_{cond}):

Unlike other gaseous systems, in the VIG the gap is evacuated to the point where the residual gas molecules will interact much more often with the glass surface than with other gas molecules (molecular flow regime). A solution of the conductance of heat in this molecular limit of gaseous surface interactions was reported by Corruccini (1959). The conductance of the residual low-pressure gas, between two parallel surfaces, is given as,

$$C_{cond} = \alpha \cdot \left[\frac{\gamma+1}{\gamma-1}\right] \cdot \left[\frac{\Re}{8 \cdot \pi \cdot M \cdot T}\right]^{\frac{1}{2}} \cdot P \tag{2.3}$$

$$B = \alpha \cdot \left[\frac{\gamma+1}{\gamma-1}\right] \cdot \left[\frac{\Re}{8 \cdot \pi \cdot M \cdot T}\right]^{\frac{1}{2}} \tag{2.4}$$

$$C_{cond} = B \cdot P$$

where:

$$\alpha = \frac{\alpha_1 \alpha_2}{\alpha_2 + \alpha_1(1-\alpha_2)}$$

α_2, α_3 = the accommodation coefficient of the gas interaction at the inner glass surfaces 2 and 3. This coefficient defines the relative energy-exchange efficiency of the interaction at the surface, and will depend on temperature, surface conditions, gas type, etc. Typically, in a VIG it is expected that α_2 and α_3 are approximately 0.89 each, resulting in a combined accommodation coefficient, α, of approximately 0.8. If a conservative value is needed then a value of 1.0 could be used since it will result in the greatest thermal conductance contribution, where all other parameters are unchanged.

γ = Specific heat ratio, $\gamma \cong 1.33$, for a water vapor and residual air mixture. Table 2 lists specific heat ratios for gas mixtures as a matter of completeness.

$\Re$ = Universal gas constant, $\Re$ = 8,314.4626 J/(kmol·K)

M = Specific Molecular Weight, M = 21.15 [kmol/kg], for a water vapor at typical RH levels and residual air mixture. Table 3 lists specific molar weights for other gas mixtures as a matter of completeness.

T = $(T_2 + T_3)/2$ [K]

P = Pressure of the gas [Pa]

From 1991 to 2005, several publications relating to VIG thermal conductance have been published. In defining the thermal conductance of the residual gas, the Corruccini (1959) work is fundamental. Equation (2.4) is a corrected, practical formulation, that applies the kinetic theory of gases to defined better the gaseous conductance between two surfaces as a function of pressure, temperature, molecular mass, and an energy exchange efficiency factor known as the accommodation coefficient. In its practical use, it is important to note that in Equation (2.4), T is not a simple average of the two boundary temperatures but an effective value derived from the kinetic energy distribution of gas molecules in a nonequilibrium state, and P the gas pressure must be interpreted at the location of thermal interaction, and not necessarily from a gauge at some other remote location in the vacuum system.

A significant contribution in Equation (2.4) is the Thermal Accommodation Coefficient (TAC), α, which quantifies the efficiency with which a gas molecule exchanges energy with a surface. The TAC is a fundamental quantity that represents critical factors affecting the conductance contribution due to the residual gas. The TAC quantifies the collision efficiency of gaseous molecular energy exchange with a solid surface. When a gas molecule strikes the surface, it may rebound retaining most of its original energy (specular reflection) or it can equilibrate to the temperature of the surface before re-emitting (diffuse reflection). The value of α ranges from 0 (purely specular) to 1 (perfectly diffuse), and it critically affects the value of gaseous heat transfer in the free molecular regime.

The fundamental physics of α is governed by kinetic gas theory, with α being a function of the incident and reflected energy distributions. The process of energy transfer, in particular, of free molecules between plane parallel surfaces, is strongly influenced by several factors:

1. **Temperature**: α generally increases at lower temperatures, as slower-moving molecules interact longer with the surface, allowing more energy exchange.

2. **Surface condition**: Rougher or contaminated surfaces (e.g., with water vapor or hydrocarbons) enhance adsorption and scattering, increasing α. In particular, roughness results in an increased number of gas-wall collisions and their angular variation.
3. **Gas species**: Lighter gases like He tend to have lower α values due to low polarizability and fast speeds, while heavier gases such as N_2 and Ar achieve higher accommodation.
4. **Material composition**: The thermal properties of the surface (e.g., SiO_2) affect how energy is absorbed and transferred back, which is attributed to physical adsorption effects.
5. **Adsorbed layers**: Even a single monolayer of adsorbed gas (e.g., water) can significantly increase α, by up to ±20%, due to enhanced interaction time and variability in scattering behavior.

In reported works, α, for Ar and N_2 on dense $CaSiO_3$ and SiO_2 material (similar surface types to float glass) was found to be close to 1 at room temperature, while α for He was found to be ~0.3. Determining correct estimates of α is essential in a VIG system because the residual gas conduction is a key thermal contribution. If α is not reasonably defined, the design of thermal performance can lead to under- or over-predicted overall thermal conductance. Moreover, an accurate analysis of the measured thermal conductance of a VIG is made difficult, where issues of vacuum instability due to outgassing, or undesirable issues of low emissivity changes, cannot be defined.

To illustrate the importance of gas composition, Table 1 shows the effective molar mass and specific heat of air across different humidity levels. Table 2 summarizes reported estimates of the TAC on glasseous surfaces.

Table 1. Effective Molar Mass and Specific Heat Ratio of Air at 25°C

Relative Humidity (%)	Molar Mass (kg/kmol)	Specific Heat Ratio (-)
0 (dry air)	28.97	1.402
20	26.77	1.386
50	23.49	1.364
80	20.19	1.342
99 (saturated)	18.12	1.327

Table 2. Reported Thermal Accommodation Coefficients (α) on Glasseous Surfaces

Gas	Surface Condition	α (Range)
Helium	Clean glass	0.01 – 0.3
Air	Standard glass (room temp)	0.8 – 1.0
Argon	Contaminated glass	0.7 – 0.9
Nitrogen	Smooth, clean glass	0.4 – 0.7
Water vapor	Humid glass	0.6 – 1.0

2.2 Thermal Conductance of Support Elements: The Pillar Array (C_{pa})

The gap between the glass panes in a VIG is maintained through a regular array of sub-millimeter sized support elements, commonly known as pillars. Typically, the pillars are cylindrical in shape and are a thermal bridge between the panes, and thus, the heat transfer through the pillars needs to be accounted for.

Typically, the cylindrical pillar is in the range of 0.3-0.5 mm in diameter and 0.1-0.2 mm in height, and are spaced 20-50 mm apart, in the form of a square or staggered array. In the following sections the analytical equations for the thermal resistance of a single pillar, for a variety of geometries, as well as for different pillar array geometries, are presented with validation.

While thermal conductance (C) is directly proportional to the overall heat transfer in a VIG, we will be discussing the inverse of thermal conductance, which is the thermal resistance, R. Conductance of the pillar array, C_{pa} is therefore:

$$C_{pa} = \frac{1}{R_{pa}}$$

Where:

$$R_{pa} = S_p^{\,2} \cdot R_p \tag{2.5}$$

R_{pa} = Thermal resistance of the pillar array [m²·K/W]

Where:

S_p = Separation between pillars in a pillar array [m]
R_p = Thermal resistance of a single pillar [m²·K/W]

The thermal resistance associated with each pillar is a combination of three independent processes,

1. **Constriction resistance [R_c]**: resistance to heat flow from the glass into the pillar, a pillar-to-glass size effect, which would be the cold side or surface 2 of the glass panes,
2. **Spreading resistance [R_s]**: resistance to heat flow from the pillar into the glass, a pillar-to-glass size effect, which would be the hot side or surface 3 of the glass panes, and
3. The 1-Dimensional **conductive heat flow resistance [R_d]** through the pillar, which is related to the material used to make the pillar.

The total resistance to heat flow of a single pillar, R_p, is obtained by combining in series the constriction, spreading, and conductive resistances:

$$R_p = R_c + R_s + R_d \tag{2.6}$$

Figure 2 is a simple illustration of the heat flow into and out of a contact interface between two semi-infinite surfaces. Here, the volumetric heat source is constrained as it flows into the interface and then spread out to fill the sink volume. The spreading/constriction resistance is directly

related to the difference in the temperature field between the source and the sink, with respect to the total heat flow into and out of the source. Numerous publications report solutions for various cases (McGee et al. 1985, McWaid and Marshall 1992, Yovanovich 1975, and Yovanovich and Michael 1967). In the case of pillars in a VIG the actual heat source is not at the contact, which results in a uniform temperature field at the contact, and a spatially varying heat flux over the contact surface. This is the defined isothermal heat flow case for an isotropic half space.

The simplest pillar configuration to consider is a cylindrical disc shape, with a finite thickness. The heat flow through such a pillar, within an array, is considered to be independent of any other pillar, which means that the separation between pillars, also known as the pillar spacing, is much larger than the pillar size. A closed form analytical solution for the constriction (and equally the spreading) resistance of a single cylindrical contact is,

$$R_c = \frac{1}{4k_{glass} \cdot r} \tag{2.7}$$

where $\boldsymbol{r}$ is the radius of the pillar and k_{glass} is the thermal conductivity of the glass. This solution is well documented and has been validated through measurements (Wilson et al. 1998). Since the contact geometry of a cylinder is the same on either end, clearly the constriction and spreading resistance should be equal: $R_c = R_s$. Where the contact geometry is not the same, the constriction/spreading resistance would be solved for the specific contact geometry.

In addition to the resistance of heat flow into and out of the pillar, there is the resistance to heat flow because of the material that the pillar is made from. This is simply the resistance to heat flow due to the conductivity, and volume, of the pillar material, which is simply given as,

$$R_d = \frac{h}{k_{pillar} \cdot A} \tag{2.8}$$

where $A = \pi r^2$ is the cross-sectional area of the cylindrical pillar, h is the height of the pillar, and k_{pillar} is the thermal conductivity of the pillar. Therefore, the total resistance to heat flow for a cylindrical pillar is, assuming the contact area on the glass surfaces is equal and that the thermal conductivity of each glass pane is different,

$$R_p = \frac{1}{4k_{glass_1} \cdot r} + \frac{1}{4k_{glass_2} \cdot r} + \frac{h}{k_{pillar} \cdot \pi \cdot r^2} \tag{2.9}$$

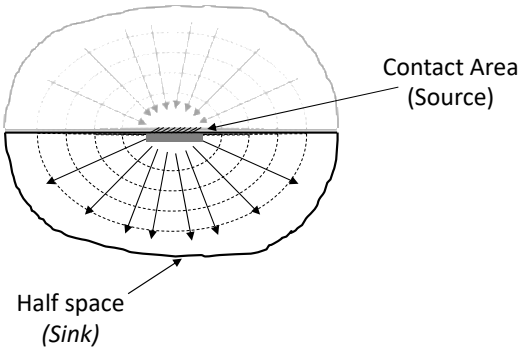

Figure 2. An illustration that highlights the constriction and spreading of heat flow isotherms through the source contact and the sink volume.

It is interesting to note that the constriction/spreading resistance, by definition, includes the thermal resistance of the glass. However, the conductivity term does not. The error that results because the glass contribution is not included in each term is small and considered to be negligible in all cases to be discussed in the following sections. The results from the equation for R_p are found to be in good agreement with guarded hot plate (GHP) measurements and finite element method (FEM) simulations: see Figure 3.

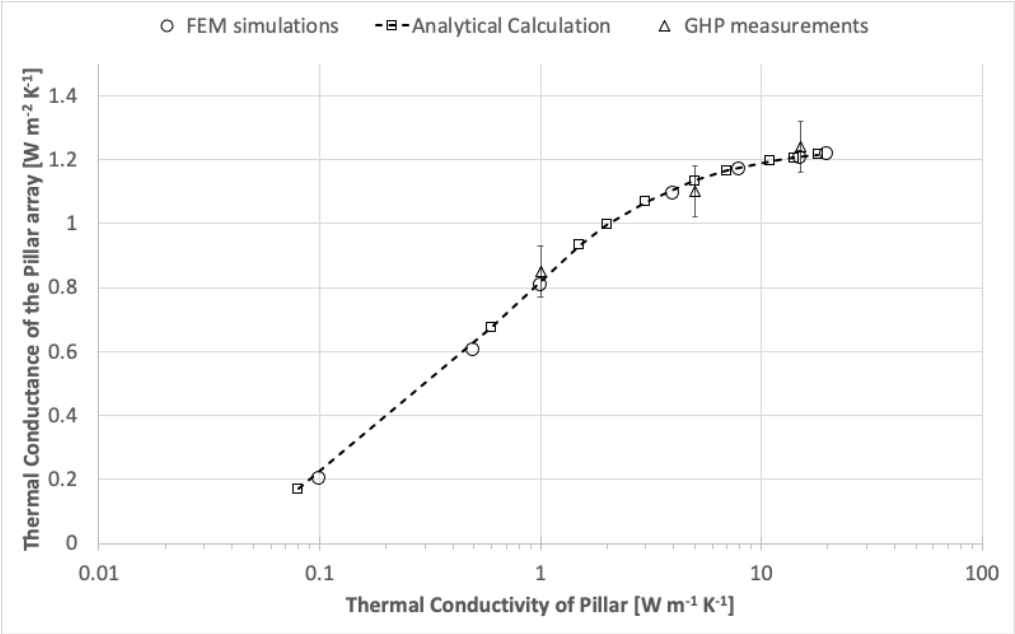

Figure 3. Plot of the thermal conductance, as a function of pillar material thermal conductivity, from the analytical solution, Equation (2.9), and compared to GHP measurements and FEM simulations. The solutions in this plot are for a pillar array separation of 20 mm, the glass thermal conductivity is taken to be 1 W/(m·K), and the pillar is 0.5 mm in diameter and 0.2 mm in height.

2.2.1 Thermal resistance of various pillar geometries

There are various geometric options for the pillar. Each geometry results in a different thermal resistance contribution. In the following sections the analytical solutions for the thermal resistance of the most common pillar geometries are presented.

The analytical results presented were validated through direct comparisons to the results obtained from numerical simulations and measurements. The numerical simulations were performed using a finite element modelling platform. In all simulations the solver type and mesh density were determined to provide convergence in the solution. To perform direct measurements, a small VIG sample, which was actively pumped (to ensure residual gas effects were negligible), was constructed with the desired pillars. Using a small area GHP, the heat flow through a single pillar was measured. Complete details of the simulation and measurement methods are not provided here as a matter of brevity and will be provided in follow-up reports, as required.

It is important to note that the thermal resistance of a contact does not change whether the contact is on surface 2 or 3 of the glass panes. Nevertheless, it is important to orientate the surfaces with respect to surface 2 and 3, since the thermal conductivity of the glass panes could be unequal. Therefore, the relevant terms of the analytical solutions are labelled with respect to the thermal conductivity of glass pane 1 (outdoor-faced) and 2 (indoor-faced).

2.2.1.1 Regular Polygon Geometries

The most common pillar geometry is the cylindrical disc shape. The well-known analytical solution for this geometry was given in Equation (2.9). The cylindrical case can be categorized along with the set of regular polygons, as illustrated in Figure 4. This means that the thermal resistance of each geometry can be related with little error by using the normalizing factor $k_{glass}\sqrt{A}$, where A is the area of contact (note – in all cases given below data are for a VIG unit where the glass panes are of identical physical and thermal properties). If we plot the total thermal resistance, R_p, as in Figure 5, the results of different geometries show good agreement.

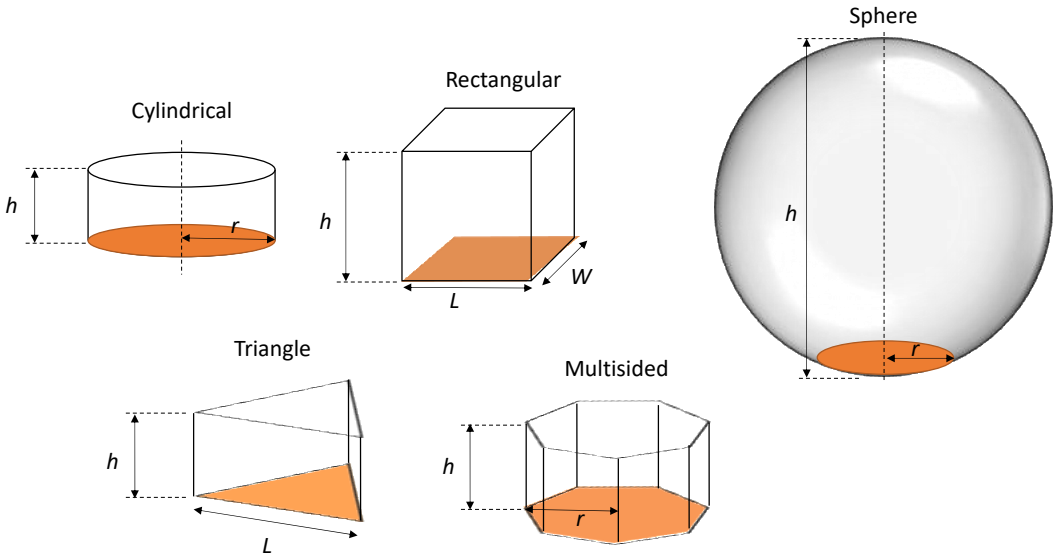

Figure 4: Illustrations of the contact area for a cylinder, sphere, and various regular polygons.

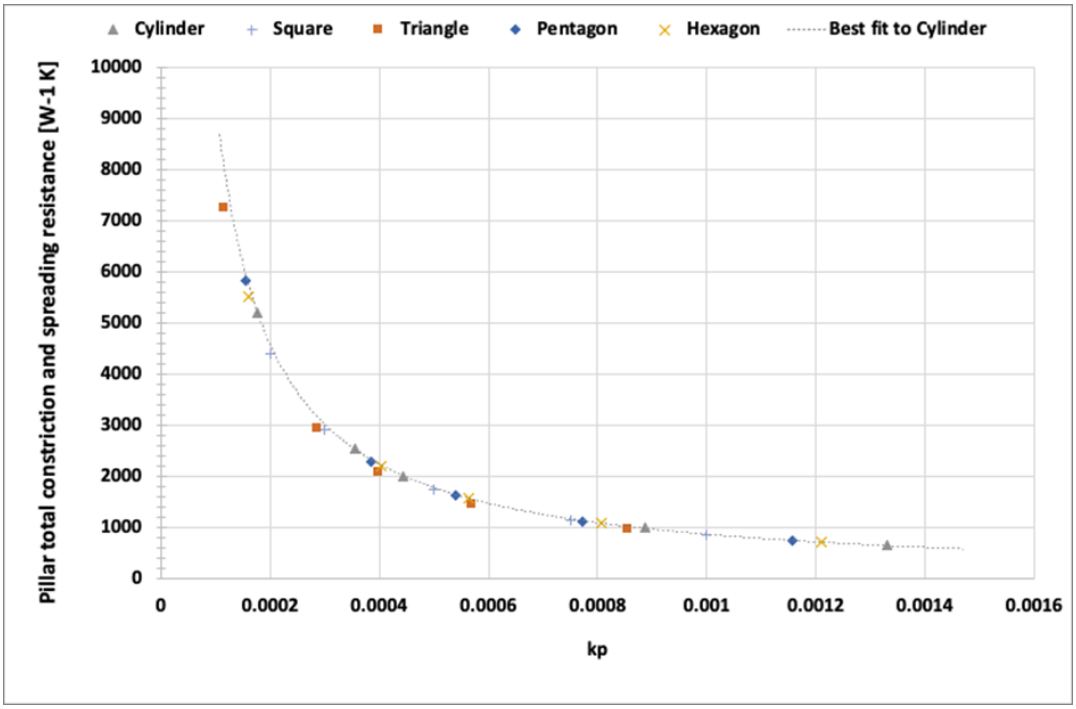

Figure 5: Plot of the total thermal resistance, R_p, as a function of the normalizing factor $k_{glass}\cdot\sqrt{A}$ from FEM simulations. The solutions in this plot are for a single pillar, where the pillar thermal conductivity is 15 W/(m·K), the glass thermal conductivity is 1 W/(m·K), and the reference cylindrical pillar is 0.5 mm in diameter and 0.2 mm in height. Other geometries were calculated for a similar overall size

This means that for the various geometries, as illustrated in Figure 4, the total thermal resistance, which includes constriction, spreading, and conduction contributions, can be given as:

$$R_p = \frac{\sqrt{\pi}}{4\cdot k_{glass_1}\cdot\sqrt{A}} + \frac{\sqrt{\pi}}{4\cdot k_{glass_2}\cdot\sqrt{A}} + \frac{h}{k_{pillar}\cdot A} \qquad (2.10)$$

where A is the area of contact, of the pillar geometry to the glass surface. In all practical cases, the contact area of the pillar will need to be determined through a direct visual measurement of pillars in a 'real' VIG unit. The actual contact area not only depends on the pillar geometry but also the deformation of the pillar which results from atmospheric pressure and the effects of the production process. The area of contact for the geometries illustrated in Figure 4 can be written as:

1. Cylindrical: $A = \pi\cdot r^2$
2. Sphere: $A = \pi\cdot r^2$
3. Rectangular: $A = L\cdot W$
4. Triangle: $A = \frac{\sqrt{3}}{4}\cdot L^2$
5. Multisided:

a. Pentagon: $A = \frac{5 \cdot \sqrt{3}}{4} \cdot r^2$

b. Hexagon: $A = \frac{3 \cdot \sqrt{3}}{4} \cdot r^2$

2.2.1.2 Linear bearing: the Elliptic Integral Solution

The linear bearing pillar is a cylinder, where its length is greater than its diameter, contacting the glass surface over its length: see Figure 6. This results in a rectangular contact area on the glass, where the final size depends highly on the undeformed size of the cylinder and the load applied to it. As mentioned in the previous section, in practical VIG units the user will need to measure directly the contact area of the pillar, since determining the contact area using an analytical solution will require knowledge of material and design parameters, which are not practical to obtain for commercial VIG products.

For a known rectangular contact area, various independent analytical solutions have been proposed. In this work the solution of the contact thermal resistance is obtained by using the known geometric functions of an Ellipse geometry. This solution was found to provide better results over a wider range of contact sizes. The detailed step-by-step formulation is not provided here, as a matter of brevity. The solution for the constriction and spreading resistance is found to be:

$$R_C = \frac{1}{4 \cdot k_{glass_1} \cdot L}\left(\frac{2}{\sqrt{\pi}} K_1\right); \; R_S = \frac{1}{4 \cdot k_{glass_2} \cdot L}\left(\frac{2}{\sqrt{\pi}} K_1\right)$$

where the main function of the Elliptic integral of the first kind is

$$K_1 = \frac{\pi\sqrt{2}}{\sqrt{m}}\left(1 - \frac{n \cdot \sqrt[4]{2}}{4 \cdot \sqrt[4]{m}}\right)$$

$$m = \left(1 + \frac{W}{L}\right) \cdot \sqrt{\frac{W}{L}}$$

$$n = 1 + \sqrt{\frac{W}{L}}$$

where L is the length and W is the width of the rectangle contact area. The conductive heat flow resistance is:

$$R_d = \frac{D}{k_{pillar} \cdot L \cdot W}$$

As mentioned previously, for pillars with symmetric contact, that is the same contact area on both top and bottom glass sheets, the constriction and spreading resistance is equal. In addition, as the heat flow enters the pillar material, spreading of the heat is negligible since the pillar height, in this case the diameter of the cylinder, is small. This means that the 1-dimensional conduction of heat

through this pillar can be calculated based on a rectangular volume of material. Therefore, the total thermal resistance associated with a single linear bearing pillar is:

$$R_P = \frac{1}{4 \cdot k_{glass_1} \cdot L}\left(\frac{2}{\sqrt{\pi}} K_1\right) + \frac{1}{4 \cdot k_{glass_1} \cdot L}\left(\frac{2}{\sqrt{\pi}} K_1\right) + \frac{D}{k_{pillar} \cdot L \cdot W} \tag{2.11}$$

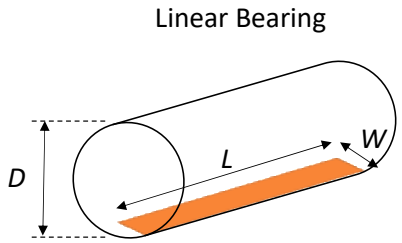

Figure 6: Illustration of the rectangular contact area obtained for a linear bearing pillar geometry

GHP measurements were performed on a limited range of sizes of the linear bearing pillar. Figure 7 is a plot of the analytic solution, simulation and GHP measurements for a linear bearing pillar. The data are labelled to highlight fixed lengths, L, since there are cases where the ratio *L/W* is equal for different lengths of linear bearing. Clearly, the calculated, simulated and measured data are in good agreement.

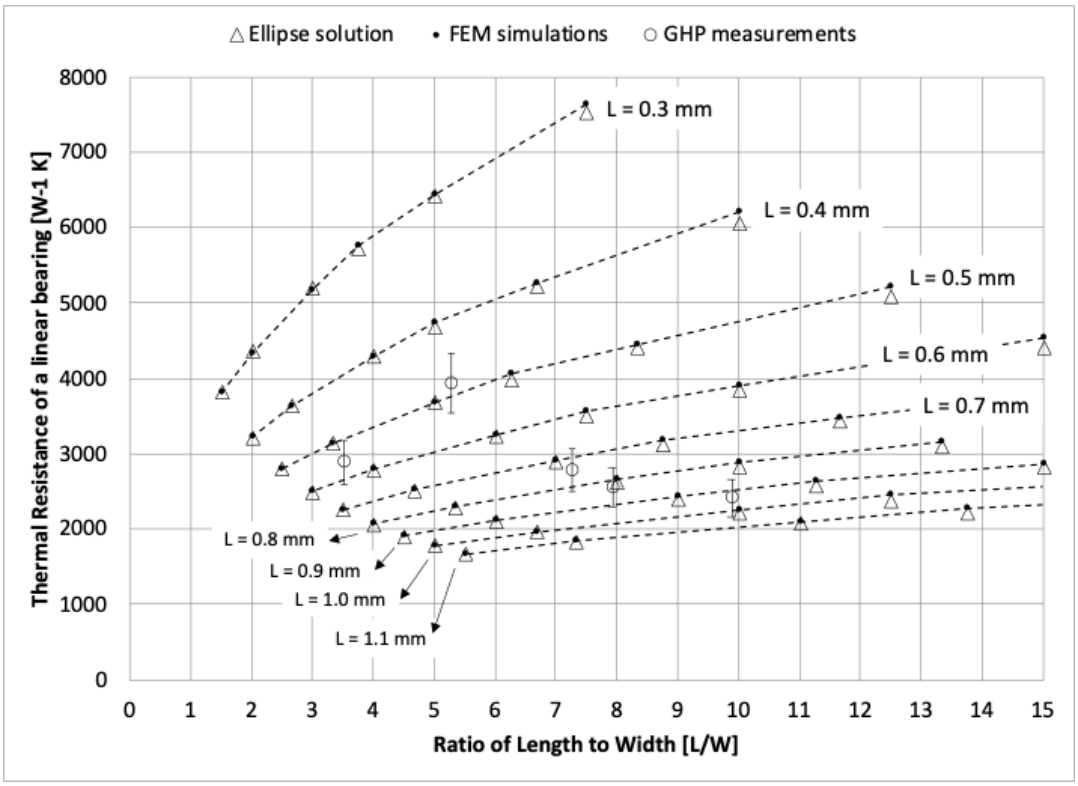

Figure 7: A plot of the linear bearing thermal resistance, as a function of the contact area length/width ratio. The solutions in this plot are for a single pillar, where the pillar thermal conductivity is 15 W/(m·K), the glass thermal conductivity is 1 W/(m·K), and the diameter of the pillar is 0.1 mm.

The ellipse solution proposed here is for a rectangular contact area, which should cover the expected solution for a rectangular pillar geometry. These solutions, however, do diverge for an L/W ratio that is large.

Figure 9 is a plot of the thermal spreading resistance of the ellipse and rectangular solutions, and highlights the percentage difference between the solutions (on the right Y-axis). For a percentage difference of 1.8% or less, the ratio of L/W should be less than 2.

This means that for a rectangular pillar geometry the following solutions should be used,

1. For $L/W < 2$, Equation (2.10)

2. For $L/W \geq 2$, Equation (2.11)

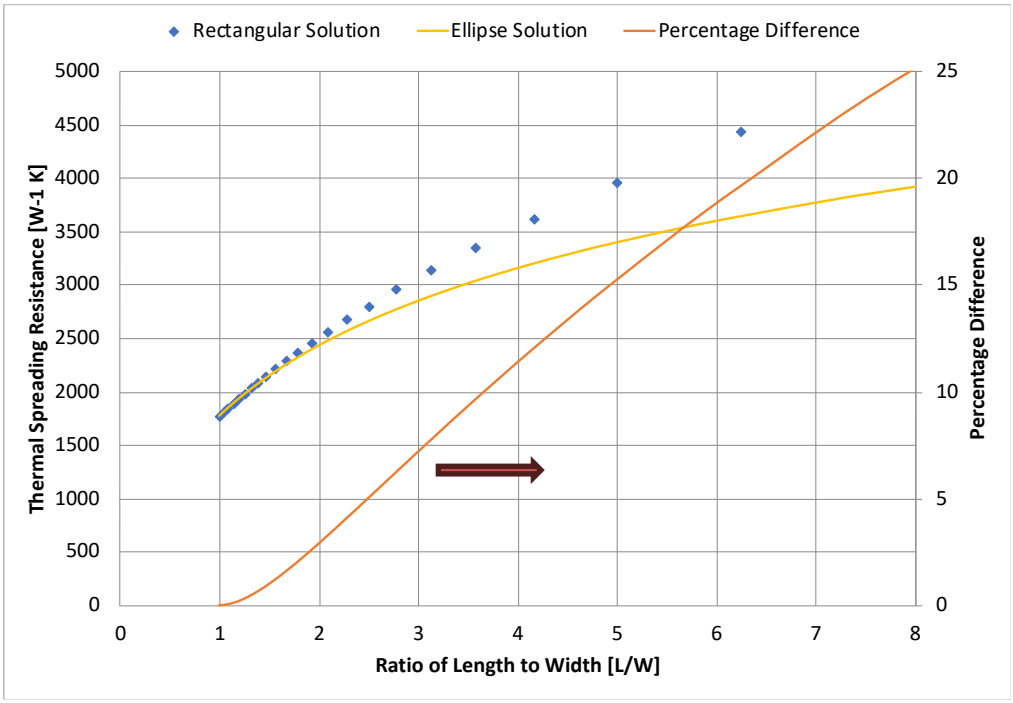

Figure 8: A plot of the thermal spreading resistance from the Ellipse and rectangular solutions (left Y-axis), with a plot of the percentage difference between the two solutions (right Y-axis), as a function of the contact area aspect ratio L/W. The pillar parameters used in this plot were the same as that given in the caption of Figure 7.

2.2.1.3 Truncated Cone

When a material deposition process of 'printing' is used to form a pillar feature on the glass surface, using glass or ceramic paste, the typical shape formed closely resembles a truncated cone: see Figure 9. In this case the contact of this geometry is asymmetric with the contact areas on the top and bottom glass not the same. The 1-Dimensional conduction resistance is specifically determined for the truncated cone for the spreading of heat within the pillar. The total thermal resistance of the truncated pillar is given in Equation (2.12), and Figure 10 shows the comparison to simulated and measured results, where the data are in good agreement. The plots are for normalized conductance, which is obtained using the normalizing factor ($k_{glass}\sqrt{A}$).

$$R_P = \frac{1}{4 \cdot k_{glass_1} \cdot r_1} + \frac{1}{4 \cdot k_{glass_2} \cdot r_2} + \frac{h}{k_{pillar} \cdot \pi \cdot r_{av}} \tag{2.12}$$

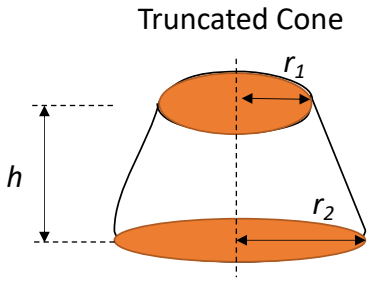

Figure 9: Illustration of the contact area for a truncated cone pillar geometry.

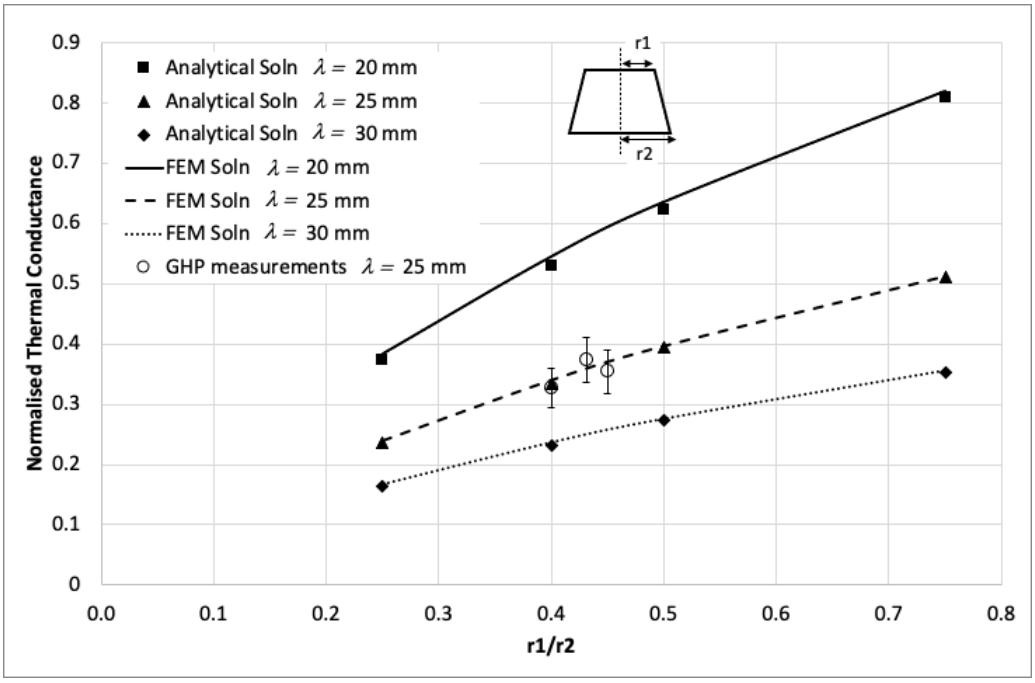

Figure 10: A plot of the normalized thermal conductance, as a function of the ratio of the top and bottom radii. The data are from the analytical solution, FEM simulations and GHP measurements. The solutions in this plot are for a single pillar, where the pillar thermal conductivity is 15 W/(m·K), the glass thermal conductivity is 1 W/(m·K), and the height of the pillar is 0.2 mm.

2.2.1.4 Annulus Cylindrical

Annulus shaped pillars, as shown in Figure 11, have been proposed in the past because of the potential to increase thermal resistance by reducing the contact area for heat flow. However, the heat flow through this pillar is not linearly related to the contact area. Therefore, a single solution for this case could not be found. Rather, two solutions valid over two independent ranges of size were formulated. The constriction resistance solutions are given as

$$1.0 < \frac{1}{\eta} \le 1.1: \quad R_C = \frac{1}{\pi^2 \cdot k_{glass_1} \cdot r_0} \left(\frac{\ln(16) + \ln\left(\frac{1+\eta}{1-\eta}\right)}{1+\eta} \right) \tag{2.13}$$

$$R_S = \frac{1}{\pi^2 \cdot k_{glass_2} \cdot r_i} \left(\frac{\ln(16) + \ln\left(\frac{1+\eta}{1-\eta}\right)}{1+\eta} \right)$$

$$1.1 < \frac{1}{\varepsilon} < \infty: \quad R_C = \frac{\pi}{8 \cdot k_{glass_1} \cdot r_0} \left(\frac{1}{\left(\cos^{-1}\eta + \sqrt{1-\eta^2} \cdot \tanh^{-1}\eta\right) \cdot \left(1 + \frac{0.0143 \cdot (\tan 1.28 \cdot \eta)^3}{\eta}\right)} \right) \tag{2.14}$$

$$R_S = \frac{\pi}{8 \cdot k_{glass_2} \cdot r_i} \left(\frac{1}{\left(\cos^{-1}\eta + \sqrt{1-\eta^2} \cdot \tanh^{-1}\eta\right) \cdot \left(1 + \frac{0.0143 \cdot (\tan 1.28 \cdot \eta)^3}{\eta}\right)} \right)$$

Where: $\eta = \frac{r_i}{r_o}$

Note - here the labels C & S correspond to the glass pane labels 1 & 2, respectively, for the contribution of Constriction and Spreading

Since the contact area of the top and bottom surfaces are equal, conductive heat flow resistance is:

$$R_d = \frac{h}{k_{pillar} \cdot A}$$

Where: $A = \pi \cdot \left(r_o^2 - r_i^2\right)$

Therefore, the total contact thermal resistance for the annulus pillar is, for the relevant range:

$$R_p = R_c + R_s + R_d \tag{2.15}$$

Figure 12 is a plot of the normalized thermal conductance, and the data are in good agreement: the data here are presented normalized as a matter of producing a plot to highlight the features of the data sets. The plots in Figure 12 are for normalized conductance, which is obtained using the normalizing factor $k_{glass} \cdot \sqrt{A}$.

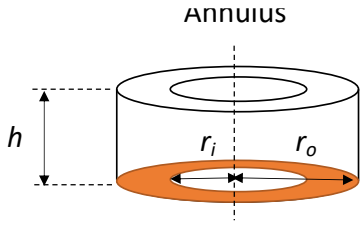

Figure 11: Illustration of the contact area of an annulus pillar geometry.

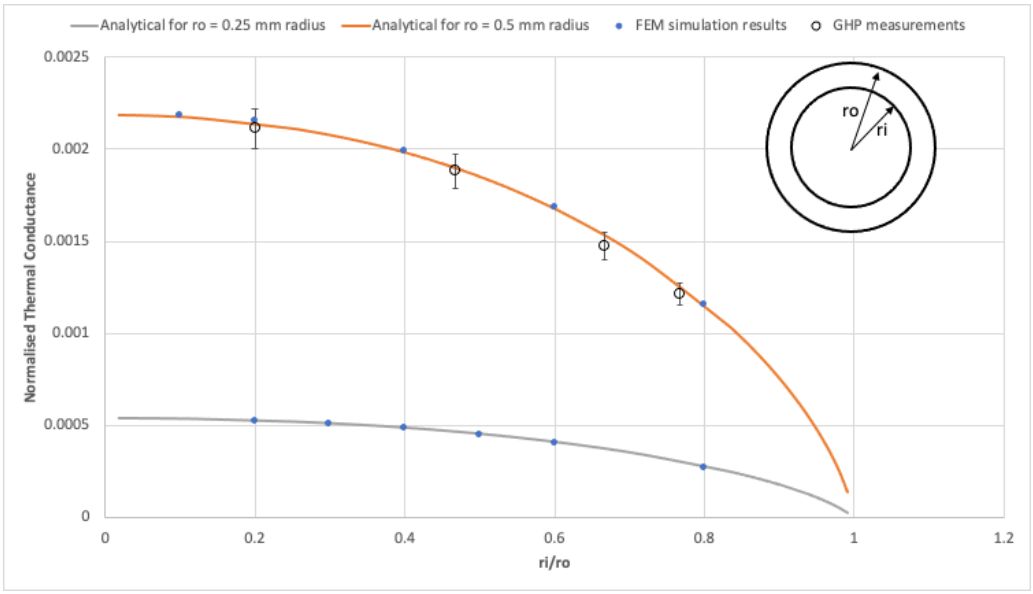

Figure 12: A plot of the normalized thermal conductance, as a function of the ratio of outside and inside radii. The data are from the analytical solution, FEM simulations and GHP measurements. The solutions in this plot are for a single pillar, where the pillar thermal conductivity is 15 W/(m·K), the glass thermal conductivity is 1 W/(m·K), and the height of the pillar is 0.2 mm.

2.2.1.5 C-shaped cylindrical

A well-known variation of the standard annulus cylindrical pillar is the C-shaped pillar, which is simply the former pillar geometry with a section, or fraction, of the material removed. This C-shaped geometry is illustrated in Figure 13, with the parameters that define the geometry highlighted.

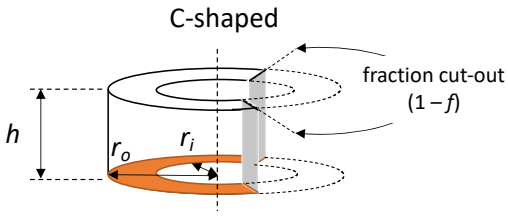

Figure 13: Illustration of the contact area of a C-shaped cylindrical pillar geometry.

The heat flow through this geometry is well described by a weighted solution of the full annulus pillar geometry, as given in Equation (2.15). Starting with the original annulus solution, and adding a factor representing the fraction of material remaining, as highlighted in Figure 13, the total thermal resistance, with respect to the original annulus solution, is written as,

$$R_p = \frac{1}{\sqrt{C_o}}\left(R_c^{annulus} + R_s^{annulus} + \frac{h}{k_{pillar} \cdot A} \right) \tag{2.16}$$

Where:

$$A = \pi \cdot \left(r_o^2 - r_i^2 \right) \cdot f$$

$$C_o = 0.94 \cdot f$$

f = fraction (between 0 and 1) of material remaining.

This analytical solution, when compared to a full 3D finite element simulations results in a maximum difference of approximately 10% at the extremes of the practical range of pillar geometries expected. The comparison of these results is shown in Figure 14.

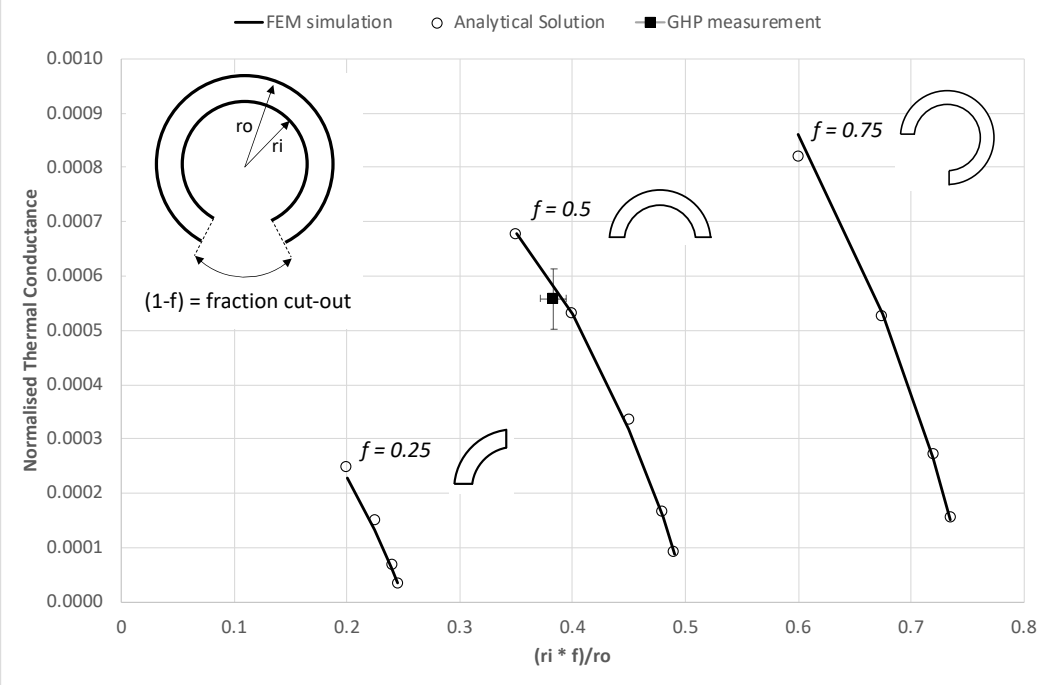

Figure 14: A plot of the normalized thermal conductance, as a function of the ratio of outside and inside radii, multiplied by the factor, *f*, which is the percentage of material remaining. The data are from the analytical solution, FEM simulations and a GHP measurement. The solutions in this plot are for a single pillar, where the pillar thermal conductivity is 15 W/(m·K), the glass thermal conductivity is 1 W/(m·K), and the height of the pillar is 0.2 mm.

2.3 Thermal Resistance of the Pillar Array

In the previous sections, the thermal resistance R_p was presented for various pillar geometries of practical interest, where the resistance is for a single pillar. In the case of a glazing/window it is the total thermal conductance of all the pillars that is of interest: that is, the thermal conductance of the pillar array. The thermal resistance of an individual pillar is associated with the unit cell of glass area. Figure 15a illustrates a typical square array, emphasizing the square-shaped unit cell of glass that covers each pillar.

In general, we define the unit cell as the area of glass where the heat flow reaches a net-zero point at the boundaries of the unit cell, effectively cancelling out the heat flow between adjacent pillars. Therefore, for a square array of pillars the thermal resistance of the pillar array, R_{pa} is given as,

$$R_{pa} = S_p^{\,2} \cdot R_p \tag{2.17}$$

where S_p is the separation between pillars in a square array.

However, practical VIG units employ various array geometries. In Figure 15, we illustrate the current practical and available array geometries, which are (a) square, (b) shifted square, and (c) shifted-rotated square configurations. These diverse geometries serve as design options to minimize the number of pillars in the VIG construction. In Figure 15 (b) and (c), we highlight the actual unit cell boundaries in green. It's evident that in these cases, the unit cell is not square, but is rather regular hexagonal in shape. To determine the unit cell shape in a VIG, the process involves identifying the net-zero heat flow boundaries between pillars. These boundaries represent surfaces across which the heat flow is balanced, resulting in no net heat transfer. To determine the net-zero heat flow surfaces, factors such as the arrangement of the pillars and the spacing between them must be observable over the glass panes.

In general, for all potential pillar array geometries, the total thermal resistance is calculable if the unit cell area is measurable, which means that

$$R_{pa} = A \cdot R_p \tag{2.18}$$

where A is area of glass over the unit cell. In general, for VIG products, the unit cell, and the area associated with the unit cell, should be determined through direct observation of the pillar array of the product, which is also the case when considering the pillar shape and size.

This means that there are three options in selecting the pillar array geometry;

1. The array geometry matches directly one of the three options of geometry highlighted in Figure 15,
2. The user has identified a unit cell configuration which is uniform over each pillar in the VIG unit, and has determined a unit cell area in the units of per m^2 or ft^2,
3. The user has identified a unit cell configuration which is uniform over each pillar in the VIG unit, and has determined the number of pillars in the VIG unit per m^2 or ft^2.

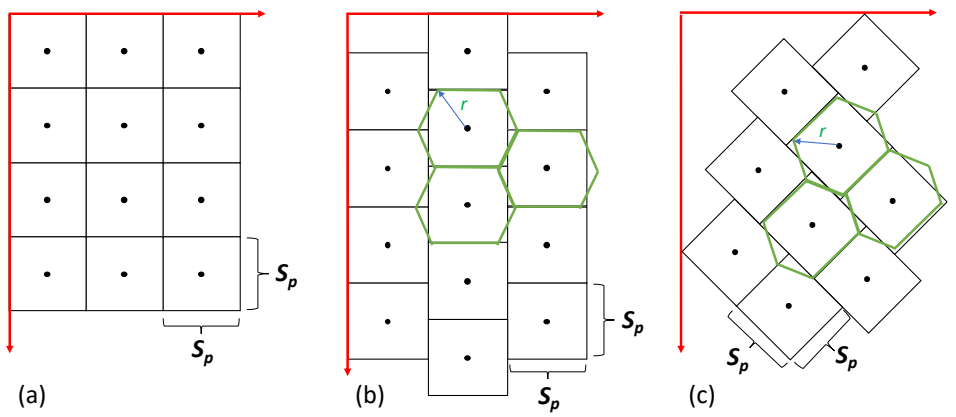

Figure 15: An illustration of pillar arrays, (a) square, (b) shifted square, and (c) shifted-rotated square, which are typical array types found in practical VIG units.

It is reasonable to expect that some VIG designs could use a non-uniform pillar application over the surface of the glass. This is the same as a pillar unit cell shape, or area, that is not equal for each pillar in the VIG. In such a case the solution of thermal conductance due to the pillars cannot be solved analytically. The user must use a more detailed numerical method to simulate the whole VIG design, to determine accurately the thermal conductance contribution. Alternatively, use the measured conductance to determine conductance of the gas and pillar array (C^*), detailed in Section 4.

2.3.1 Thermal Conductance of surface-to-surface Radiation (C_{rad})

A significant contribution to the overall thermal conductance of a VIG is the surface-to-surface radiation over the internal gap, between surface 2 and 3. Radiative conductance between two parallel plates is given by,

$$C_{rad} = \varepsilon_{eff} \cdot \sigma \cdot \frac{\left(T_3^4 - T_2^4\right)}{T_3 - T_2} \tag{2.19}$$

where:

$$\varepsilon_{eff} = \frac{1}{\frac{1}{\varepsilon_2} + \frac{1}{\varepsilon_3} - 1}$$

and where:

ε_{eff} = effective emissivity of surfaces 2 and 3 (infinite parallel plates), [-]

ε_2 = emissivity of the first facing glass surface, surface 2, [-]

ε_3 = emissivity of the second facing glass surface, surface 3, [-]

σ = Stefan-Boltzmann Constant, 5.67 x 10^{-8}, [W/(m^2·K^4)]

T_2 = Temperature of the first facing glass surface, surface 2, [K]

T_3 = Temperature of the second facing glass surface, surface 3. [K]

Equation (2.19) is a precise formulation for two parallel plates at constant temperature, nevertheless, it can be simplified to use the average temperature between the glass panes,

$$C_{rad} = 4 \cdot \varepsilon_{eff} \cdot \sigma \cdot T_m^{\,3} \tag{2.20}$$

where T_m is the mean temperature between surface 2 and 3, [K]

$$T_m = \frac{T_2 + T_3}{2}$$

3. The total center-of-glass, air-to-air, U-factor of the VIG (U_{VIG})

The U-Factor of the VIG, U_{VIG}, is air-to-air thermal transmittance. It includes surface heat transfer coefficients at the indoor and outdoor glazing surfaces – surfaces 1 and 4. and is calculated similarly to the standard method used for a conventional IGU, except that in a conventional IGU the gap conductance is calculated from the set of equations for natural convection of a gas-fill (e.g., Air, Argon, Krypton) in rectangular tall cavity, $h_{c,i}$ and surface-to-surface radiation consisting of radiant heat fluxes (i.e. radiosities) leaving the front and back facing glass surfaces, $J_{f,i}$ and $J_{b,i}$. In terms of these variables the heat flux across the i^{th} gap (i.e. q_i) is:

$$q_i = h_{c,i} \cdot \left(T_{f,i} - T_{b,i-1}\right) + J_{f,i} - J_{b,i-1}$$

For VIG units, convection/conduction heat transfer in the gap needs to be replaced by C^*. as follows:

$$h_{c,i} = C_i^*$$

So, for VIG, the following is the expression for heat flux:

$$q_i = C^* \cdot \left(T_{f,i} - T_{b,i-1}\right) + J_{f,i} - J_{b,i-1} \tag{3.1}$$

The rest of the model and full system of equations for the N glazing layers is described in WINDOW Technical Documentation (Curcija et al. 2018)

3.1 Simplified VIG U-Factor Calculation

Simplified model, convenient for quick calculations of the thermal transmittance of double-glazing, is given below.

$$U = \frac{1}{R_{tot}} = \frac{1}{R_o + R_{glass_1} + R_{gap} + R_{glass_2} + R_i} \tag{3.2}$$

$$R_{gap} = \frac{1}{C_{gap}} \tag{3.3}$$

For VIG, C_{gap} is calculated according to equation (2.1).

$$R_{glass} = \frac{t_{glass}}{k_{glass}} \tag{3.4}$$

Where:

t_{glass} = glass thickness [m]

k_{glass} = glass conductivity [W/(m·K)]

R_o = Outdoor surface heat transfer resistance, calculated using ISO (2007) [m²K/W].

R_i = Indoor surface heat transfer resistance, calculated using ISO (2007) [m²K/W].

Note: For NFRC boundary conditions, approximate values for R_o and R_i are $R_o \approx 0.034$ m²K/W and $R_i \approx 0.147$ m²K/W

4. Calculation of Thermal Transmittance from Measured Data (C^*)

When details of gap space pressure and/or pillars are not known or are uncertain the conductance of the pillars and the residual gas only, or conductance of the gap space without the surface-to-surface radiation contribution, C^* can be calculated using the measured conductivity of the VIG, k_{VIG} (e.g., ASTM 2021).

$$C^* = \frac{1}{R_{gap}} - C_{rad} \tag{4.1}$$

Where:

R_{gap} is derived from the measured conductivity k_{VIG}, VIG overall thickness t_{VIG}, and thicknesses and conductivities of each glass layer, t_{g1}, k_{g1}, t_{g2}, k_{g2}.

$$R_{gap} = R_{VIG} - \left(R_{glass1} + R_{glass2} \right) \tag{4.2}$$

Where:

$$R_{VIG} = \frac{1}{C_{VIG}}$$

$$C_{VIG} = \frac{k_{VIG}}{t_{VIG}}$$

Therefore:

$$R_{VIG} = \frac{t_{VIG}}{k_{VIG}}$$

$$R_{g1} = \frac{t_{glass1}}{k_{glass1}}$$

$$R_{g2} = \frac{t_{glass2}}{k_{glass2}}$$

Substituting R_{VIG} and R_{g1}, R_{g2} into Equation (4.2), R_{gap} becomes:

$$R_{gap} = \frac{t_{VIG}}{k_{VIG}} - \left(\frac{t_{glass1}}{k_{glass1}} + \frac{t_{glass2}}{k_{glass2}} \right) \tag{4.3}$$

Substituting equation (4.3) for R_{gap} and equation (2.19) for C_{rad} into equation (4.1), the following equation is obtained for calculating C*:

$$C^* = \frac{1}{\frac{t_{VIG}}{k_{VIG}} - \left(\frac{t_{glass1}}{k_{glass1}} + \frac{t_{glass2}}{k_{glass2}} \right)} - \frac{\sigma}{\frac{1}{\varepsilon_1} + \frac{1}{\varepsilon_2} - 1} \cdot \left(\frac{T_3^4 - T_2^4}{T_3 - T_2} \right) \tag{4.4}$$

Where temperatures T_2 and T_3 are calculated from the measured heat flux and known temperatures T_1, and T_4, which are surface temperatures applied at the cold and hot plates during the measurement. The following equalities assume that the heat flow into surface 4 is equal to the heat flow out of surface 1 (1-D heat flow assumption), where the heat flux is measured and expressed in terms of k_{VIG}, t_{VIG} and temperature differential ($T_4 - T_1$):

$$q_1 = q_4 = q = \frac{k_{VIG}}{t_{VIG}} \cdot (T_4 - T_1)$$

At the same time, q_1 and q_4 can be expressed as heat transfer across the glass layers (again, utilizing 1-D heat flow assumption):

$$q_1 = \frac{k_{g1}}{t_{g1}} \cdot (T_2 - T_1) \Rightarrow T_2 = \frac{t_{g1}}{k_{g1}} \cdot q_1 + T_1$$

$$q_4 = \frac{k_{g2}}{t_{g2}} \cdot (T_4 - T_3) \Rightarrow T_3 = T_4 - \frac{t_{g2}}{k_{g2}} \cdot q_2$$

Therefore:

$$T_2 = \frac{t_{glass1}}{k_{glass1}} \cdot \frac{k_{VIG}}{t_{VIG}} \cdot (T_4 - T_1) + T_1 \tag{4.5}$$

$$T_3 = T_4 - \frac{t_{glass2}}{k_{glass2}} \cdot \frac{k_{VIG}}{t_{VIG}} \cdot \left(T_4 - T_1\right) \tag{4.6}$$

This equation works only if glass 1 and glass 2 have thermal IR transmittance equal to zero. For non-zero IR transmittance, this model is not applicable.

5. References

ASTM. 2021. "C518 - Standard Test Method for Steady-State Thermal Transmission Properties by Means of the Heat Flow Meter Apparatus". ASTM International.

Corruccini, R.J. 1959. "Gaseous Heat Conduction at Low Pressures and Temperatures" *Journal Vacuum*. Vol. VII.

Curcija, D.C; Vidanovic, S.; Hart, R.; Jonsson, J.; Powles, R.; and Mitchell, R. 2018. "WINDOW Technical Documentation". LBNL Technical Report. Lawrence Berkeley National Laboratory. April 2018.

ISO. 2007. "ISO 15099 – Thermal performance of windows, doors and shading devices — Detailed calculations". International Standardization Organization.

Kristiansson, Simon, Fredrik Ingvarson, and Kjell O. Jeppson. "Compact spreading resistance model for rectangular contacts on uniform and epitaxial substrates. *IEEE transactions on electron devices.* Pp. 2531-2536.

McGee, G. R., M. H. Schankula, and M. M. Yovanovich. 1985. "Thermal resistance of cylinder-flat contacts: Theoretical analysis and experimental verification of a line-contact model. Nuclear Engineering and Design. Pp. 369-381.

McWaid, T., and E. Marschall. 1992. "Thermal contact resistance across pressed metal contacts in a vacuum environment. *International journal of heat and mass transfer*. Pp. 2911-2920.

Wilson, C. F., T. M. Simko, and R. E. 1998. Collins. "Heat conduction through the support pillars in vacuum glazing." *Solar Energy*. Pp. 393-406.

Yovanovich, M. Micheal. 1967. "Thermal contact resistance across elastically deformed spheres. *Journal of Spacecraft and Rockets.* pp 119-122.

Yovanovich, M. 1975. "Thermal constriction resistance of contacts on a half-space-Integral formulation. *10th Thermophysics Conference*.